

# Exponential Fluctuations in the Modes of Orthogonal Polarization in Pulsar Radio Emission

M. M. MCKINNON<sup>1</sup>

<sup>1</sup>*National Radio Astronomy Observatory, Socorro, NM 87801 USA*

## ABSTRACT

A statistical model for the polarization of pulsar radio emission is enhanced to account for the heavy modulation of the emission, the possible covariance of the Stokes parameters, and the observed asymmetries in the distributions of total intensity, polarization, and fractional polarization by treating the intensities of the orthogonal polarization modes as exponential random variables. The model is used to derive theoretical distributions to compare with what is observed. The resulting distributions are unimodal and generally asymmetric. The unimodality arises from the model's fundamental assumption that the orthogonal modes are superposed. The asymmetry originates primarily from different fluctuations in mode intensities. The distributions of fractional polarization are truncated at the degree of linear and circular polarization intrinsic to the modes. A number of observable parameters that quantify the statistical properties of the emission and its polarization are derived and are shown to be functions only of the ratio of the modes' mean intensities,  $M$ , suggesting their spectra coevolve according to the frequency dependence of  $M$ . This particular implementation of the model requires the modes to fluctuate differently in order to replicate the observations. Since a single underlying emission mechanism seems unlikely to selectively modulate the mode intensities, the different fluctuations are attributed either to different emission mechanisms for the modes or to mode-dependent propagation or scattering effects in the pulsar magnetosphere.

## 1. INTRODUCTION

Single pulse polarization observations of pulsars are made in an attempt to understand their radio emission mechanism and the propagation of radio waves in their magnetospheres. The observations reveal the emission is highly linearly polarized and heavily modulated, often switching randomly between orthogonally polarized states (Manchester, Taylor, & Huguenin 1975; Cordes, Rankin, & Backer 1978, hereafter CRB; Stinebring et al. 1984a, hereafter S84a). The orthogonal polarization modes (OPMs) can be elliptically polarized with each mode preferring a particular sense of circular polarization. The results of these observations have historically been presented as color-coded or grey-scale histograms of fractional linear polarization, fractional circular polarization, and polarization position angle at multiple locations across a pulsar's pulse (e.g. CRB, S84a). A number of factors can affect the appearance of the histograms, such as how the modes interact (e.g. do they occur simultaneously or separately?), the statistical character of their fluctuations, the degree and ellipticity of their polarization, and the level of instrumental noise. These factors must be understood in order for the histograms to be properly interpreted.

McKinnon & Stinebring (1998, hereafter MS1) developed a statistical model for the OPMs in pulsar radio emission. The model provides a general statistical framework for deriving the distributions of total intensity, polarization, fractional polarization, and polarization position angle given the distributions of the mode intensities. They proposed the emission consists of two independent, completely linearly polarized, simultaneously occurring, orthogonal modes of polarization. The model treats the mode intensities as random variables (RVs) to account for the emission’s variability. Subsequent work accounted for the circular polarization of the modes (McKinnon & Stinebring 2000, hereafter MS2; McKinnon 2002, hereafter M02). In their detailed implementation of the model, MS1 assumed the mode intensities were Gaussian RVs. While the distributions they derived were qualitatively similar to what is observed, the implementation did not address the heavy modulation of the observed emission, incorporate the possible covariance of the Stokes parameters, or replicate some asymmetries observed in distributions of the Stokes parameters and fractional polarization. For example, if the total intensity of the emission follows Gaussian statistics, the ratio of its standard deviation to its mean (the modulation index,  $\beta$ ) must be  $\beta < 0.2 - 0.3$  for the intensity to be positive definite (M02). However, observed modulation indices are often much larger, sometimes exceeding unity (e.g. Bartel, Sieber, & Wolszczan 1980, hereafter BSW). The implementation should accommodate large values of  $\beta$  because OPMs tend to occur where the emission is heavily modulated (McKinnon 2004, hereafter M04). MS1 also assumed the standard deviations of the Gaussian mode intensities were equal thereby stipulating the Stokes parameters (specifically I and Q in their analysis) were also independent RVs. This assumption simplified the derivation of the distribution of fractional polarization. In general, the Stokes parameters are covariant (MS1), and a more robust implementation of the model should provide for the correlation. The assumption of Gaussian mode intensities always produces Gaussian, and thus symmetric, distributions of the Stokes parameters and Gaussian-like distributions of fractional polarization (MS1; M02). While similar distributions are observed, other distributions have shapes that are more complex or asymmetric.

The purpose of this paper is to incorporate the heavy modulation of the emission, provide for the covariance of the Stokes parameters, and replicate asymmetries in the observed distributions of the Stokes parameters and fractional polarization by assuming the mode intensities are exponential, instead of Gaussian, RVs in the model’s implementation. An exponential RV has the property that its mean and standard deviation are equal, and its modulation index is consequently equal to one. The assumption of exponential mode intensities also results in the Stokes parameters generally being covariant. Asymmetries in distributions of the Stokes parameters and fractional polarization arise from the different statistical properties of the exponential mode intensities.

The paper is organized as follows. The general framework of the MS1 statistical model is briefly reviewed in §2. The framework is used to derive the distributions of total intensity, linear polarization, fractional linear polarization, and polarization position angle when the mode intensities are exponential RVs. Parameters are derived to quantify the statistical properties of the emission and its polarization. The implementation is then extended to include circular polarization and to account for instrumental noise. In §3, a numerical simulation of the model is used to replicate observed distributions of fractional polarization and position angle in PSR B1929+10 and PSR B2020+28. A comparison is made between the results obtained from the model’s treatment of exponential and Gaussian RVs in §4. The implications of the analysis for the generation of OPMs and the frequency dependence of the emission and its polarization are also discussed.

## 2. POLARIZATION STATISTICAL MODEL

### 2.1. Model Overview

The MS1 statistical model for the polarization of pulsar radio emission is reviewed here for convenience and reference for the sections that follow. The simplest form of the model proposes that the polarization of the emission is determined by the incoherent superposition of two completely linearly polarized, orthogonal modes. The model is consistent with the theoretical proposition that OPMs are the natural modes of wave propagation in the pulsar magnetosphere (Melrose 1979; Onishchenko 1981; Allen & Melrose 1982; Barnard & Arons 1986). The model accounts for the stochastic nature of OPMs by representing their flux densities by the RVs  $X_1$  and  $X_2$ , which are distributed according to the functions,  $f_1$  and  $f_2$ , respectively. The RVs have means  $\mu_j$  and standard deviations  $\sigma_j$ . The primary mode is designated as  $X_1$  ( $\mu_1 > \mu_2$ ), and  $X_2$  is the secondary mode. Since the modes are incoherent, they propagate independently, and the total intensity of the combined emission is the sum of the mode flux densities (Chandrasekhar 1960). To simplify the analysis, but without loss of generality, a polarization position angle of  $\psi = 0$  is assigned to the primary mode, and a position angle of  $\psi = \pi/2$  is assigned to the secondary mode. So defined, the vectors representing the mode polarizations are antiparallel to one another and form a diagonal along the Q-axis in the Poincaré sphere. Since the polarization vectors are antiparallel, the amplitude of the resultant polarization vector is the difference between the mode polarization amplitudes, and the tip of the vector resides in one hemisphere of the Poincaré sphere or the other depending upon which mode is instantaneously the stronger of the two. With these assumptions and definitions, the Stokes parameter I of the combined emission is the sum of the mode intensities,  $I = X_1 + X_2$ , and the Stokes parameter Q is their difference,  $Q = X_1 - X_2$ . The remaining Stokes parameters are  $U = V = 0$ . The amplitude of the linear polarization is  $L = |Q|$ . General expressions for the probability distributions of I, Q, and L can be derived from these definitions of the Stokes parameters (MS1).

$$f_I(x) = f_1 * f_2 \quad (1)$$

$$f_Q(x) = f_2 \star f_1 \quad (2)$$

$$f_L(x) = f_2 \star f_1 + f_1 \star f_2 \quad (3)$$

The asterisk in equation 1 denotes convolution, and the stars in equations 2 and 3 denote correlation. In this idealized model, the distribution of polarization position angle consists of two delta functions separated by  $\pi/2$  radians. The frequency of occurrence of the primary mode (the amplitude of the larger delta function) is the probability that the Stokes parameter Q exceeds zero.

$$\nu_1 = \int_0^\infty f_Q(x) dx \quad (4)$$

Instrumental noise has been ignored in the derivation of equations 1-4, but is incorporated in the analysis in §2.5.

### 2.2. Distributions from Exponential Mode Intensities

In their detailed implementation of the polarization model's statistical framework, MS1 assumed the mode intensities,  $X_1$  and  $X_2$ , were Gaussian RVs. Their analysis is repeated here, but with the mode intensities taken to be exponential RVs. The distribution of an exponential RV is given by

$$f_j(x) = \frac{1}{\mu_j} \exp(-x/\mu_j), \quad x \geq 0, \quad (5)$$

where the subscripts  $j = 1, 2$  denote the primary and secondary modes, respectively. The distributions of I and Q can be found by inserting the exponential distributions,  $f_1$  and  $f_2$ , from equation 5 into equations 1 and 2.

$$f_I(x) = \frac{1}{\mu_1 - \mu_2} [\exp(-x/\mu_1) - \exp(-x/\mu_2)], \quad x \geq 0 \quad (6)$$

$$f_Q(x) = \begin{cases} \frac{1}{\mu_1 + \mu_2} \exp(-x/\mu_1), & x \geq 0, \\ \frac{1}{\mu_1 + \mu_2} \exp(x/\mu_2), & x < 0. \end{cases} \quad (7)$$

Similarly, from equations 3 and 5, the distribution of linear polarization is

$$f_L(x) = \frac{1}{\mu_1 + \mu_2} [\exp(-x/\mu_1) + \exp(-x/\mu_2)], \quad x \geq 0. \quad (8)$$

From equations 4 and 7, the frequency of occurrence of the primary mode in the position angle distribution is

$$\nu_1 = \frac{M}{M+1}, \quad (9)$$

where  $M = \mu_1/\mu_2$  is the ratio of the mode mean intensities. The frequency of occurrence of the secondary mode is  $\nu_2 = 1 - \nu_1 = 1/(M+1)$ , and the relative frequency of occurrence of the modes is  $\nu_1/\nu_2 = M$ . The mean of Stokes Q normalized by the mean total intensity,  $m$ , is equal to the difference between the frequencies of occurrence of the modes (i.e. the difference between the amplitudes of the two delta functions comprising the position angle distribution).

$$m = \frac{\mu_Q}{\mu_I} = \frac{\mu_1 - \mu_2}{\mu_1 + \mu_2} = \nu_1 - \nu_2 = \frac{M - 1}{M + 1} \quad (10)$$

The joint probability density of Q and I is needed to derive the distribution of fractional linear polarization. The detailed procedure for deriving the joint probability density and the distribution of fractional polarization is given in the Appendix. The resulting distribution of fractional linear polarization is

$$f_{ml}(z) = \frac{(1 - m^2)(1 + m^2 z^2)}{(1 - m^2 z^2)^2}, \quad 0 \leq z \leq 1. \quad (11)$$

When the mean intensities of the modes are equal,  $\mu_1 = \mu_2 = \mu$ , the total intensity follows a gamma distribution, the linear polarization is exponentially distributed, the fractional linear polarization is

uniformly distributed, and the two delta functions in the position angle distribution have equal amplitudes ( $\nu_1 = \nu_2 = 1/2$ ).

$$f_I(x) = \frac{x}{\mu^2} \exp(-x/\mu), \quad x \geq 0 \quad (12)$$

$$f_L(x) = \frac{1}{\mu} \exp(-x/\mu), \quad x \geq 0 \quad (13)$$

$$f_{ml}(z) = 1, \quad 0 \leq z \leq 1 \quad (14)$$

### 2.3. Model Statistical Parameters

A number of parameters can be derived from the definitions of the Stokes parameters and their distributions to quantify the statistical properties of the emission and its polarization. The modulation index of the total intensity is the ratio of its standard deviation to its mean.

$$\beta = \frac{\sigma_I}{\mu_I} = \frac{(\mu_1^2 + \mu_2^2)^{1/2}}{\mu_1 + \mu_2} = \frac{(M^2 + 1)^{1/2}}{M + 1} \quad (15)$$

The Stokes parameters I and Q are generally covariant. The I-Q correlation coefficient is

$$r_{IQ} = \frac{\text{Cov}(I, Q)}{\sigma_I \sigma_Q} = \frac{\mu_1^2 - \mu_2^2}{\mu_1^2 + \mu_2^2} = \frac{M^2 - 1}{M^2 + 1}. \quad (16)$$

The mean linear polarization is

$$\mu_L = \int_0^\infty x f_L(x) dx = \frac{\mu_1^2 + \mu_2^2}{\mu_1 + \mu_2}, \quad (17)$$

and the mean linear polarization normalized by the mean total intensity is

$$\bar{L} = \frac{\mu_L}{\mu_I} = \frac{M^2 + 1}{(M + 1)^2}. \quad (18)$$

Lastly, the mean of the distribution of fractional linear polarization is

$$ml = \int_0^1 z f_{ml}(z) dz = 1 + \frac{1 - m^2}{2m^2} \ln(1 - m^2), \quad 0 < m < 1. \quad (19)$$

The statistical parameters are summarized in Table 1 and shown in Figure 1. Interestingly, all of them are functions only of the ratio of the modes' mean intensities,  $M$ , and are independent of the individual values of  $\mu_1$  and  $\mu_2$ . The parameters' sole dependence upon  $M$  arises because all parameters were derived by taking ratios of various combinations of means and standard deviations, and an exponential RV possesses the properties that its distribution is characterized by a single quantity,  $\mu$ , and its mean and standard deviation are equal. All of the parameters are, in principle, observable quantities. When  $M = 1$ , Figure 1 shows the modes occur with equal frequency ( $\nu_1 = 1/2$ ), the Stokes parameters I and Q are not correlated ( $r_{IQ} = 0$ ), the modulation index is  $\beta = 1/\sqrt{2}$ , the normalized mean of Stokes Q is  $m = 0$ , and  $\bar{L} = ml = 1/2$ . As  $M$  becomes large, all of the parameters approach unity. This behavior results from the emission being dominated by the primary

**Table 1.** Model Statistical Parameters

Parameter	Expression
Normalized Mean Q, $m$	$(M - 1)/(M + 1)$
Normalized Mean L, $\bar{L}$	$(M^2 + 1)/(M + 1)^2$
Primary Mode Frequency of Occurrence, $\nu_1$	$M/(M + 1)$
Mean Fractional Linear Polarization, $ml$	$1 + \frac{1-m^2}{2m^2} \ln(1 - m^2)$
I-Q Correlation Coefficient, $r_{IQ}$	$(M^2 - 1)/(M^2 + 1)$
Intensity Modulation Index, $\beta$	$(M^2 + 1)^{1/2}/(M + 1)$

mode. In this case, the Stokes parameters I and Q are highly correlated, and the emission is highly polarized and heavily modulated. The primary mode frequency of occurrence,  $\nu_1$ , and the intensity modulation index,  $\beta$ , closely track one another at large  $M$  with a localized slope varying as  $\sim 1/M^2$ . The parameters  $m$  and  $\bar{L}$  also track one another, but with a localized slope varying as  $\sim 2/M^2$ . The modulation index remains large for all values of  $M$ . Close inspection of the table entries reveals relationships between the parameters, e.g.  $\bar{L} = \beta^2 = \nu_1^2 + \nu_2^2 = m/r_{IQ}$ .

#### 2.4. Including Circular Polarization

The statistical model can be expanded to include circular polarization by assuming the orthogonal modes are completely elliptically polarized, in which case the Stokes parameters Q, U, and V of the combined emission are (M04)

$$Q = \sin \theta_o \cos \phi_o (X_1 - X_2), \quad (20)$$

$$U = \sin \theta_o \sin \phi_o (X_1 - X_2), \quad (21)$$

$$V = \cos \theta_o (X_1 - X_2). \quad (22)$$

Here,  $\phi_o$  is the azimuth of the primary mode's polarization vector in the Poincaré sphere and  $\theta_o$  is its colatitude. Since each mode is assumed to be completely polarized,  $\sin \theta_o$  is a mode's degree of linear polarization and  $\cos \theta_o$  is its degree of circular polarization. The definition of the Stokes parameter I remains unchanged. With these definitions, the distributions of Q, U, and V are simply scaled versions of the distribution for Stokes Q given by equation 7. To simplify the derivation of fractional linear polarization, and again without loss of generality, the azimuth of the polarization vector can be assumed to be  $\phi_o = 0$ , so that the linear polarization fluctuations are concentrated in Stokes Q,

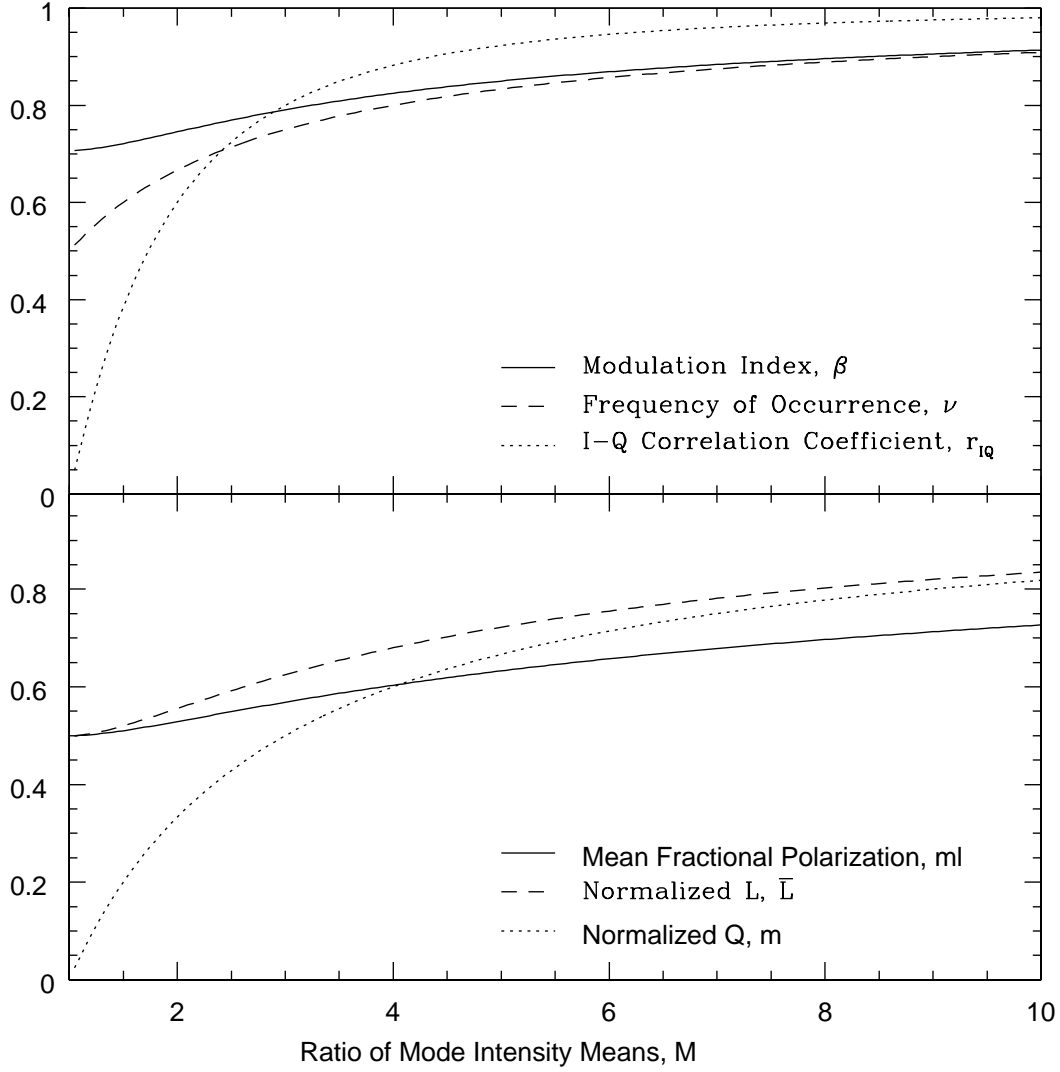


**Figure 1.** Dependence of model statistical parameters upon the ratio of mode mean intensities,  $M$ . The top panel shows how the intensity modulation index, primary mode frequency of occurrence, and correlation coefficient between the Stokes parameters I and Q vary with  $M$ . The bottom panel shows the dependence of the mean of the fractional linear polarization distribution, the normalized linear polarization, and the normalized Stokes parameter Q upon  $M$ .

as was done in §2.2. Following the analysis described in the Appendix, the distributions of fractional linear polarization,  $f_{ml}$ , and fractional circular polarization,  $f_{mv}$ <sup>1</sup>, can be shown to be

$$f_{ml}(z) = \frac{1 - m^2}{\sin \theta_o} \frac{1 + (mz/\sin \theta_o)^2}{[1 - (mz/\sin \theta_o)^2]^2}, \quad 0 \leq z \leq \sin \theta_o \quad (23)$$

<sup>1</sup> The variable  $z$  is used interchangeably to represent fractional linear polarization and fractional circular polarization in equation 23, equation 24, and Figure 2.

$$f_{\text{mv}}(z) = \frac{1}{2 \cos \theta_o} \frac{1 - m^2}{[1 - (mz / \cos \theta_o)]^2} \quad -\cos \theta_o \leq z \leq \cos \theta_o \quad (24)$$

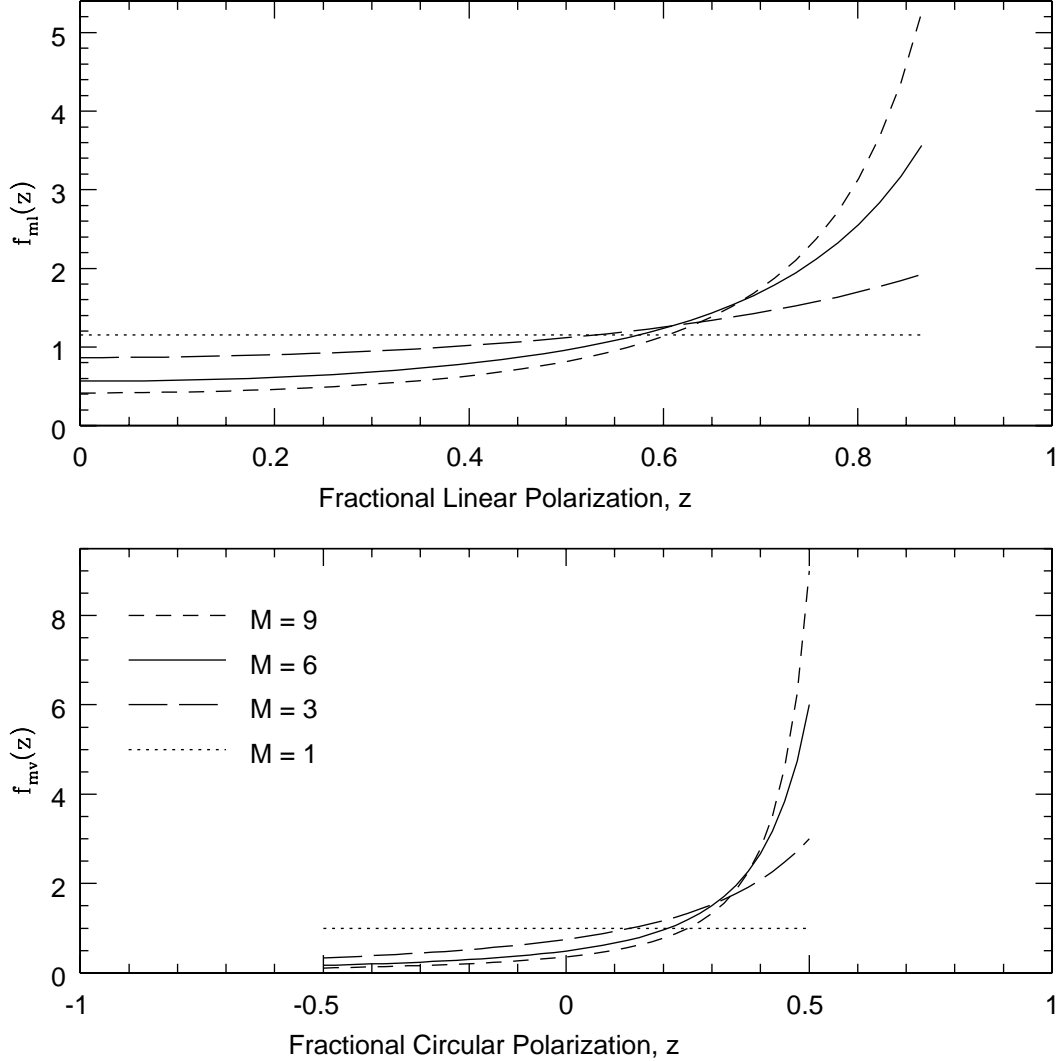


**Figure 2.** Example distributions of fractional linear polarization (top panel) and fractional circular polarization (bottom panel) when the mode intensities are exponential random variables. The distributions are shown for different values of  $M$  when  $\theta_o = \pi/3$  radians.

Example distributions of fractional polarization are shown in Figure 2 for different values of  $M$ . The distributions are generally skewed towards large values of fractional polarization, and particularly so for large values of  $M$ . The skewness, or asymmetry, of the circular distribution can be acute, with values ranging from  $1/(2M \cos \theta_o)$  at  $-\cos \theta_o$ , to  $M/(2 \cos \theta_o)$  at  $\cos \theta_o$ . The skewness of both distributions is due to the primary mode dominating the polarization of the combined emission. The distributions of fractional linear and circular polarization are also abruptly truncated at  $\sin \theta_o$ .

and  $\pm \cos \theta_o$ , respectively. The truncations highlight the fact that the fractional linear or circular polarization of the combined emission can never exceed the degree of linear or circular polarization intrinsic to an individual mode. Consequently, the ranges of the fractional polarization distributions are anti-correlated, e.g. the distribution of fractional circular polarization is narrow when the distribution of fractional linear polarization is wide, and vice versa.

The mean of the distribution of fractional circular polarization is

$$mv = \cos \theta_o \left[ \frac{1}{m} + \frac{1 - m^2}{2m^2} \ln \left( \frac{1 - m}{1 + m} \right) \right], \quad 0 < m < 1. \quad (25)$$

The mean of the distribution of fractional linear polarization is simply the result given by equation 19 multiplied by  $\sin \theta_o$ . The equations for mean fractional polarization are not valid for  $m = 0$  ( $M = 1$ ). In that particular case, the distributions of fractional polarization are uniform, the mean value of the fractional linear polarization is  $ml = \sin \theta_o/2$ , and the mean value of the fractional circular polarization is  $mv = 0$ .

### 2.5. Accounting for Instrumental Noise

The ideal distributions of the Stokes parameters derived in §2.2 are those that are intrinsic to the pulsar, at least within the context of the model. The distributions that are actually observed are affected by the additive and statistically independent instrumental noise. The effect of the noise can be significant because the narrow bandwidths and short sampling intervals used historically in single pulse polarization observations can lead to high instrumental noise. The observed distributions of the Stokes parameters are the intrinsic ones convolved with a zero-mean Gaussian representing the instrumental noise. The solution to the convolution is identical to that for the temporal broadening of a Gaussian-shaped radio pulse due to multi-path scattering from a thin screen in the interstellar medium (McKinnon 2014, hereafter M14). When the pulsar-intrinsic total intensity is exponentially distributed, the observed total intensity distribution is the convolution of equation 5 with the Gaussian instrumental noise (see equation 4 of M14)

$$f_I(x, \mu) = \frac{1}{2\mu} \exp \left( \frac{\sigma^2}{2\mu^2} \right) \exp \left( -\frac{x}{\mu} \right) \left[ 1 + \operatorname{erf} \left( \frac{x - \sigma^2/\mu}{\sigma\sqrt{2}} \right) \right], \quad (26)$$

where  $\operatorname{erf}(x)$  is the error function and  $\sigma$  is the magnitude of the instrumental noise. When the emission is comprised of the two OPMs and  $\mu_1 \neq \mu_2$ , the distribution of the observed total intensity is the convolution of equation 6 with Gaussian noise (see equation 13 of M14)

$$g_I(x) = \frac{\mu_1 f_I(x, \mu_1) - \mu_2 f_I(x, \mu_2)}{\mu_1 - \mu_2}, \quad (27)$$

where  $f_I(x, \mu)$  is given by equation 26. When  $\mu_1 = \mu_2 = \mu$ , the distribution of the observed total intensity is the convolution of equation 12 with Gaussian noise (see equation 15 of M14)<sup>2</sup>.

$$h_I(x) = \frac{\sigma}{\mu^2 \sqrt{2\pi}} \exp \left( -\frac{x^2}{2\sigma^2} \right) + \frac{(x - \sigma^2/\mu)}{\mu} f_I(x, \mu) \quad (28)$$

<sup>2</sup> Although equation 28 appears to be different from equation 15 in M14, both equations produce the same result. Equation 28 is the more concise expression of the two.

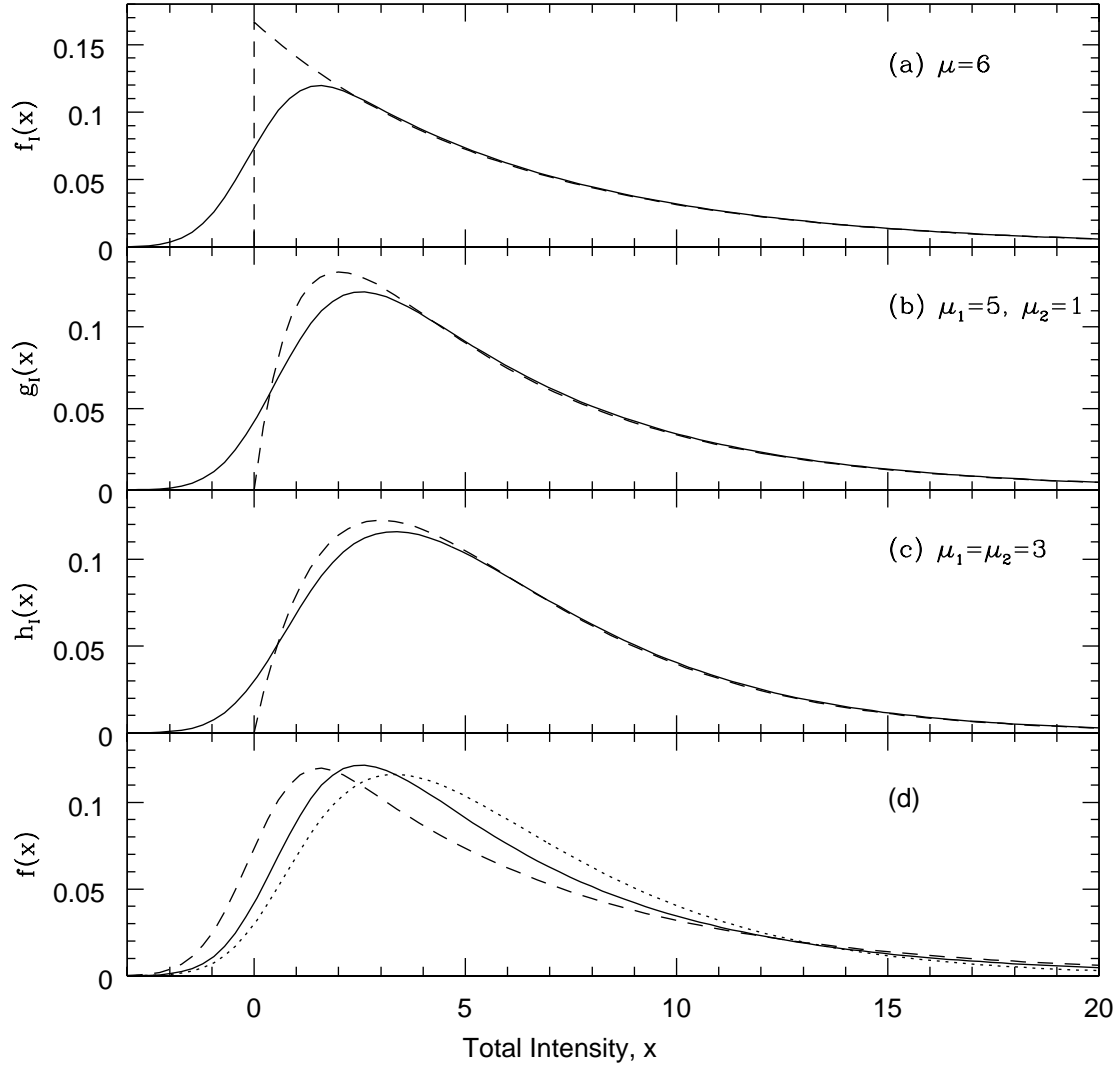


**Figure 3.** Comparisons between total intensity distributions with instrumental noise (solid line) and without noise (dashed line). Panel (a) shows the distributions when the total intensity is exponentially distributed (equations 5 & 26 with  $\mu = 6$ ). Panel (b) shows the distributions when the mode intensities are exponentially distributed, but with different means ( $\mu_1 = 5$  and  $\mu_2 = 1$ ; equations 6 & 27). Panel (c) shows the distributions when the mode intensities are exponentially distributed with identical means ( $\mu_1 = \mu_2 = 3$ ; equations 12 & 28). Panel (d) compares the three distributions that include noise from panels (a) through (c). The value of instrumental noise used in the figure is  $\sigma = 1$ ; therefore, the values on the figure's abscissa may be interpreted as a signal-to-noise ratio. All distributions in the figure have the same mean,  $\mu_1 = 6$ .

A comparison between the total intensity distributions with and without instrumental noise is shown in Figure 3. The observed distribution of the Stokes parameter  $Q$  is the convolution of equation 7 with Gaussian noise.

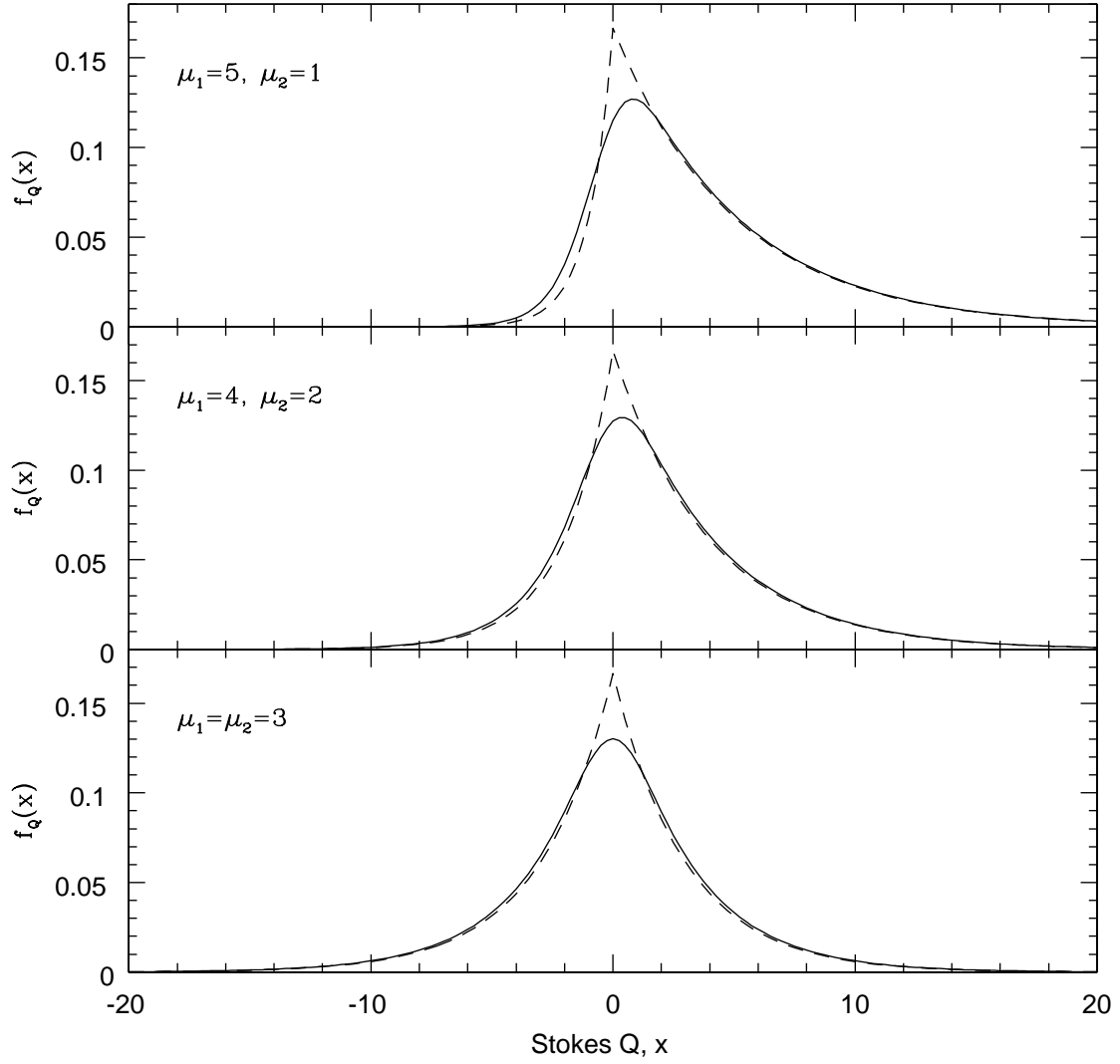


**Figure 4.** Comparisons between distributions of the Stokes parameter  $Q$  with instrumental noise (solid line) and without noise (dashed line). Each panel compares equation 7 to equation 29 using the noted values of  $\mu_1$  and  $\mu_2$ . The value of instrumental noise used in the figure is  $\sigma = 1$ .

$$f_Q(x) = \frac{1}{2(\mu_1 + \mu_2)} \left\{ \exp\left(\frac{\sigma^2}{2\mu_1^2}\right) \exp\left(-\frac{x}{\mu_1}\right) \left[ 1 + \operatorname{erf}\left(\frac{x - \sigma^2/\mu_1}{\sigma\sqrt{2}}\right) \right] \right. \\ \left. + \exp\left(\frac{\sigma^2}{2\mu_2^2}\right) \exp\left(\frac{x}{\mu_2}\right) \left[ 1 - \operatorname{erf}\left(\frac{x + \sigma^2/\mu_2}{\sigma\sqrt{2}}\right) \right] \right\} \quad (29)$$

A comparison between the distributions of the Stokes parameter  $Q$  with and without instrumental noise is shown in Figure 4. If the radio emission is circularly polarized, its distribution will be a scaled version of equation 29 and what is shown in Figure 4.

The distributions of linear polarization and position angle are derived from the joint probability density of the Stokes parameters  $Q$  and  $U$  (MS1). As the model has been constructed, the pulsar's polarization signal is completely contained within the Stokes parameter  $Q$ . The Stokes parameter  $U$  consists of instrumental noise that is independent of Stokes  $Q$ . Therefore, the joint probability density of  $Q$  and  $U$  is the product of their individual distributions ( $f_{QU} = f_Q f_U$ ). The distribution of  $Q$  is given by equation 29, and the distribution of  $U$  is a zero-mean Gaussian with noise  $\sigma$ . After converting the Cartesian coordinates of  $Q$  and  $U$  in the joint density to the polar coordinates of radius and azimuth, the azimuth distribution,  $f_\phi(\phi)$ , is found by integrating the joint density over radius. The linear polarization distribution,  $f_L(r)$ , is found by integrating the joint density over azimuth. The joint probability density is

$$f(r, \phi) = \frac{1}{2(\mu_1 + \mu_2)} \frac{r}{\sigma\sqrt{2\pi}} \times \left\{ \exp \left\{ -\frac{r^2}{2\sigma^2} \left[ 1 - \left( \cos(\phi) - \frac{\sigma^2}{\mu_1 r} \right)^2 \right] \right\} \left\{ 1 + \operatorname{erf} \left[ \frac{r(\cos(\phi) - \sigma^2/\mu_1 r)}{\sigma\sqrt{2}} \right] \right\} + \exp \left\{ -\frac{r^2}{2\sigma^2} \left[ 1 - \left( \cos(\phi) + \frac{\sigma^2}{\mu_2 r} \right)^2 \right] \right\} \left\{ 1 - \operatorname{erf} \left[ \frac{r(\cos(\phi) + \sigma^2/\mu_2 r)}{\sigma\sqrt{2}} \right] \right\} \right\}. \quad (30)$$

Since azimuth and position angle are related by  $\phi = 2\psi$ , the position angle distribution is  $f_\psi(\psi) = 2f_\phi[2(\psi - \psi_o)]$ , where  $\psi_o$  is the position angle of the primary mode polarization vector. The joint density as written in equation 30 places the mode peaks at  $\phi = 0, \pi$  in the azimuth distribution ( $\psi = 0, \pi/2$  in the position angle distribution). The primary mode peak can be arbitrarily relocated by selecting a value of  $\psi_o$ , thereby rotating the shape of the distribution in angle.

The integration of equation 30 was performed numerically for different values of  $\mu_1$  and  $\mu_2$  to generate the example distributions of position angle shown in Figure 5. The top panel of the figure shows example distributions when the mode mean intensities are equal. The two peaks representing the modes in the distributions are separated by  $\pi/2$  radians and occur with equal frequency. The amplitudes of the peaks increase and their widths narrow as the value of  $\mu$  increases. The “noise floor” across the distribution is suppressed as  $\mu$  increases. The bottom panel of the figure shows the distributions when the mode mean intensities are not equal. The amplitude of the primary mode peak exceeds that of the secondary mode. The difference between the peak amplitudes increases as  $\mu_1$  becomes larger with respect to  $\mu_2$ . The distributions in both panels of the figure resemble the analytical result derived for Gaussian RVs (see Figure 2 of MS1).

The overall shapes of the resultant distributions of linear polarization are generally similar for different values of mode mean intensities (Figure 6). They resemble a Rician distribution, but with highly extended tails. The tail extends further with increasing  $M$ . The resemblance to a Rician distribution arises from the  $r \exp(-r^2)$  dependence of the joint probability density shown in equation 30. For a comparison with the distribution of instrumental noise, a pure Rician (Rayleigh) distribution representing the noise contains most data samples within  $r = 3$  and peaks at  $r = 1$ , where  $f_L(r) = 0.607$  is off scale in the figure.

### 3. POLARIZATION SIMULATIONS

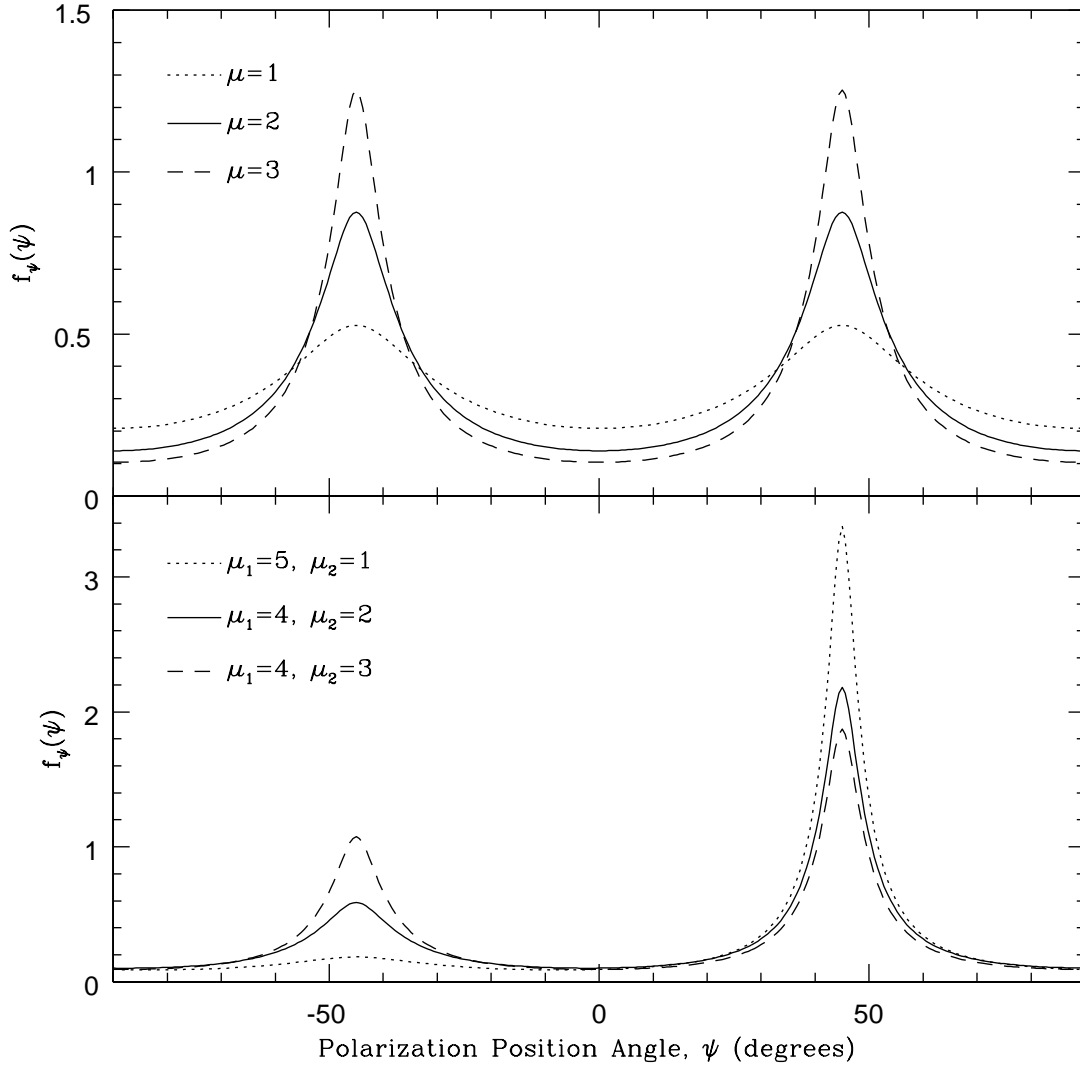


**Figure 5.** Example distributions of polarization position angle for exponentially-distributed mode intensities. In the top panel, the mean intensities of the modes are equal; their values are annotated in the panel. In the bottom panel, the mode mean intensities are not equal; their values are also listed in the panel. For presentation purposes, the position angle distribution has been rotated to place the primary mode peak at  $\psi_o = \pi/4$ . The value of instrumental noise used in the figure is  $\sigma = 1$ .

Numerical simulations were made with the statistical model to replicate observed histograms of position angle and fractional circular polarization in PSR B1929+10 at 1404 MHz (Figures 23 and 24, respectively, on page 266 of S84a) and the fractional circular polarization in PSR B2020+28 at 800 MHz (Figure 13 on page 286 of Stinebring et al. 1984b, hereafter S84b). The modes were modelled as exponential RVs. An independent Gaussian noise component with  $\sigma = 1$  was generated for each Stokes parameter. The Stokes parameters were calculated from the equations given in §2.4. The arbitrary value of the primary mode's position angle was set to  $\pi/4$ , primarily for display purposes. The remaining free parameters in the simulation are  $\mu_1$ ,  $\mu_2$ , and  $\theta_o$ . The simulation

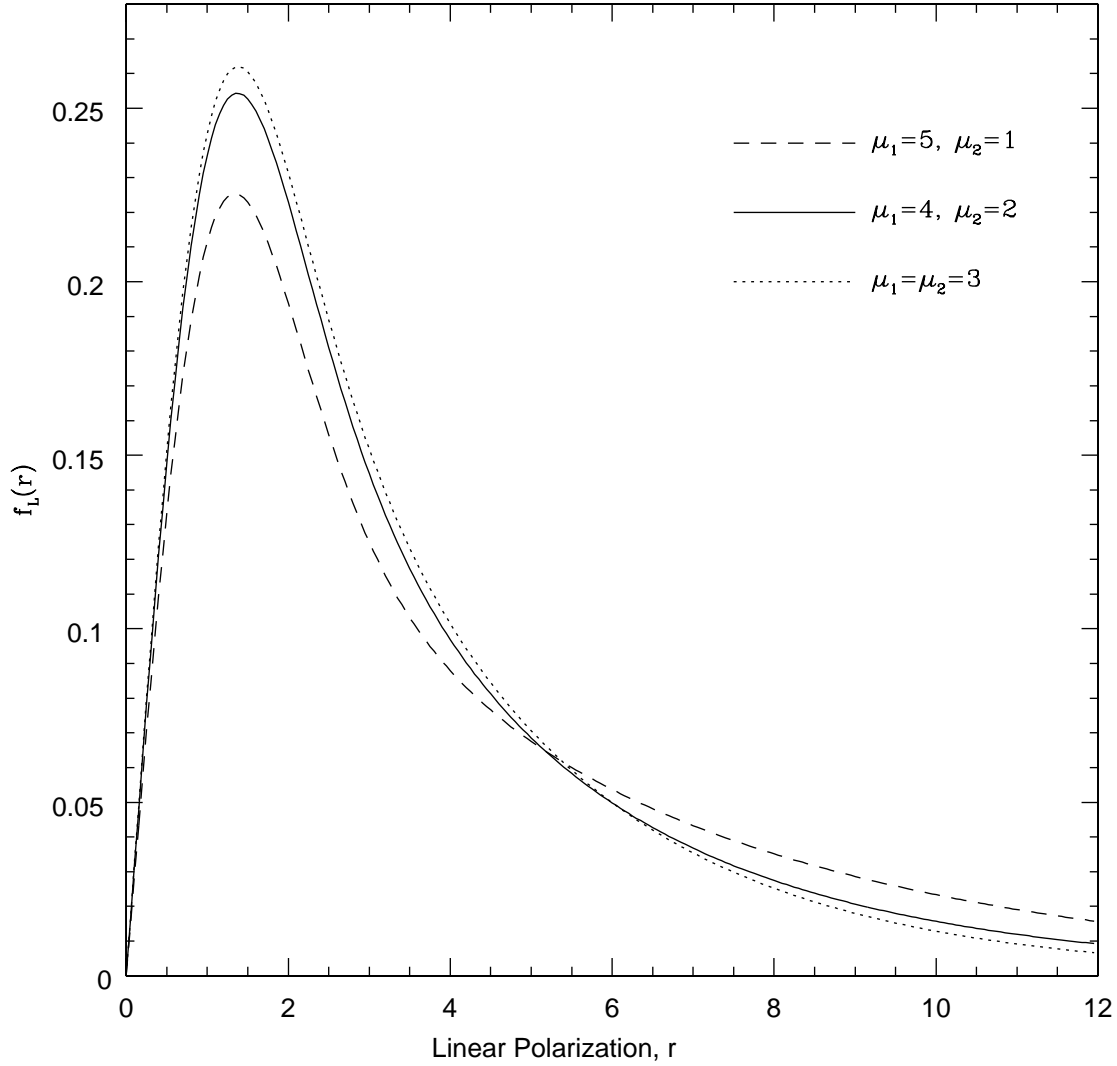


**Figure 6.** Example distributions of linear polarization for exponentially-distributed mode intensities. The values of the mode mean intensities are listed in the figure. The value of instrumental noise used in the figure is  $\sigma = 1$ .

generated 3,000 samples of each Stokes parameter. Values of fractional linear polarization, fractional circular polarization, and position angle were then calculated from the Stokes parameters and binned into histograms of 50 bins each. No detection thresholds were placed on the total intensity or linear polarization prior to constructing the histograms. The results of the simulations are shown in Figure 7.

The data used to construct the observed histograms of PSR B2020+28 were recorded near the peak of the trailing component in its pulse (S84b), where OPMs are obvious and the emission is heavily modulated ( $\beta \simeq 1.1 - 1.3$ ; see Figure 2 of M04). The pulsar is well known for the correlation between the handedness of its circular polarization and position angle at this location within its pulse (CRB; S84a). S84b noted the histogram of fractional circular polarization (Figure 13 therein) is highly

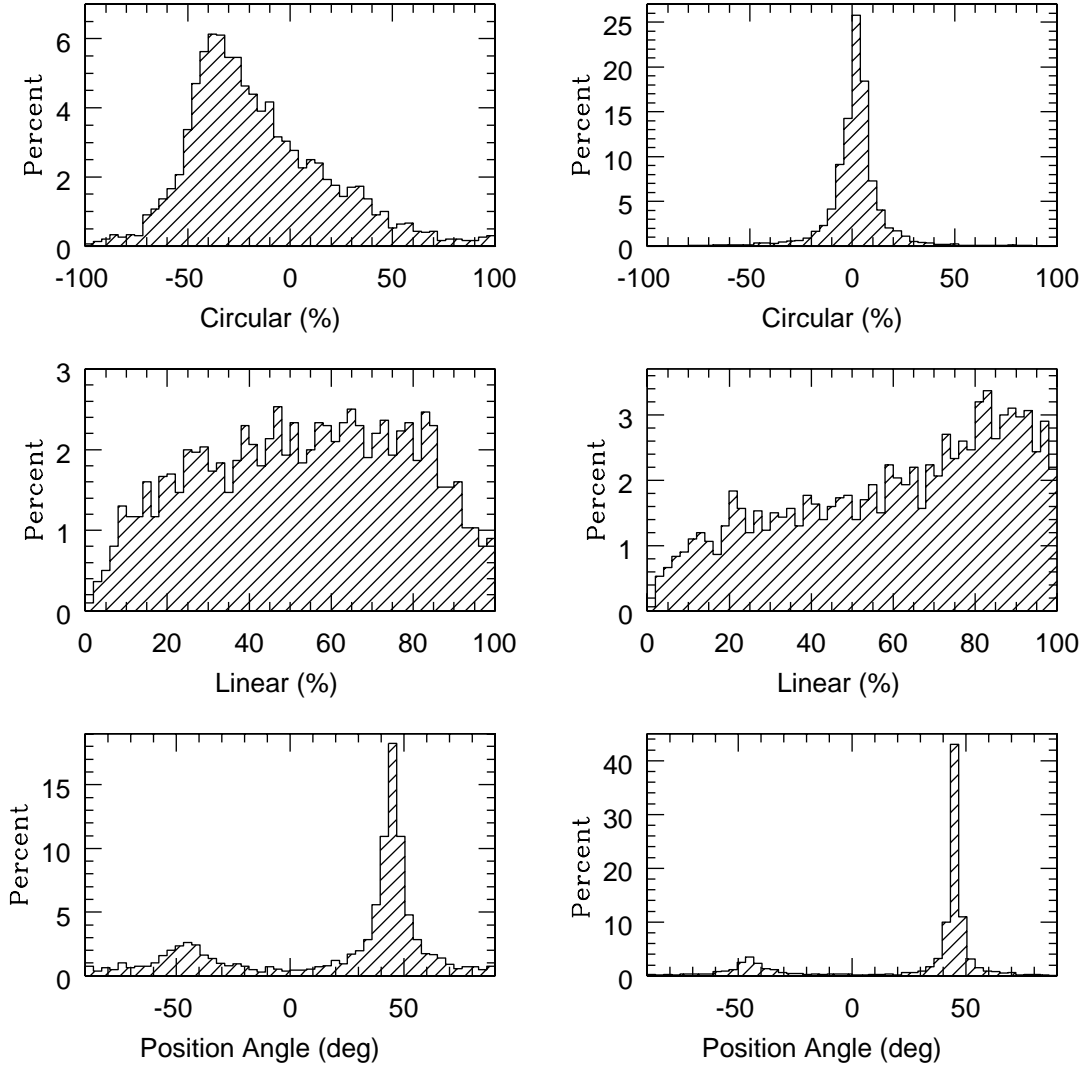


**Figure 7.** Simulated histograms of percentage circular and linear polarization and position angle. The left column of panels attempts to replicate distributions observed in PSR B2020+28 at 800 MHz (S84b). The parameters used in the simulation are  $\mu_1 = 6$ ,  $\mu_2 = 2$ ,  $\theta_o = 117^\circ$ , and  $\sigma = 1$ . The right column of panels attempts to replicate distributions in PSR B1929+10 at 1404 MHz (S84a). The parameters used in the simulation are  $\mu_1 = 15.9$ ,  $\mu_2 = 3.7$ ,  $\theta_o = 88^\circ$ , and  $\sigma = 1$ .

asymmetric with a peak near  $z = -0.3$ . More specifically, the histogram has a sharp edge at about  $z = -0.4$  with a tail extending well into positive values of fractional circular polarization. They suggested the histogram could be composed of two offset Gaussian components, with each produced by one of the modes. They correctly noted that if this were the case, the mode polarizations would not be orthogonal. A different interpretation of the histogram is it arises from the superposition of elliptically polarized orthogonal modes, and the edge of the histogram is set by the fractional circular polarization intrinsic to the modes, as shown by equation 24 and Figure 2. The simulation of PSR B2020+28 is shown in the three panels on the left side of Figure 7. The model parameters used in

the simulation are  $\mu_1 = 6$ ,  $\mu_2 = 2$ , and  $\theta_o = 117^\circ$ . The simulated histogram of fractional circular polarization generally mimics what is observed, suggesting that non-orthogonal elliptical modes are not required to explain the observation. The value of  $\theta_o$  used in the simulation indicates the degree of circular polarization intrinsic to the primary mode is  $\cos(117^\circ) = -0.45$ , which is consistent with the prevalence of strong circular polarization observed in the pulsar. The observed histogram of fractional linear polarization in Figure 12 of S84b extends to  $z \simeq 0.8$ , while the simulated histogram shows a drop off starting at about  $z = 0.85$ . The drop off is caused by the limit on the fractional linear polarization imposed by the modes at  $\sin(117^\circ) = 0.89$ . The simulated histogram of position angle appears to be a reasonable approximation to what is shown in Figure 12 of S84b.

The data used to construct the observed histograms of PSR B1929+10 were recorded on the trailing edge of the pulse peak (S84a), where OPMs are obvious and the emission is heavily modulated ( $\beta \simeq 0.6-0.7$ ; see Figure 2 of M04). The peaks in the observed position angle histogram (Figure 23 of S84a) were the narrowest of the pulsars S84a observed, with the primary mode accounting for almost 44 percent of the data samples recorded. The clear definition of the position angle peaks and the large amplitude of the primary mode peak suggest a significant difference between the mode means. Despite the high linear polarization implied by the position angle histogram, Figure 22 on page 267 of S84a shows the fractional linear polarization of the pulsar at this location spans the entire range of possible values ( $0 \leq z \leq 1$ ). The observed histogram of fractional circular polarization (Figure 24 therein) is very narrow with a large peak at zero and a slight asymmetry composed of a steep edge at positive polarization and a subtle tail at negative polarization. The occurrence of completely polarized samples in the observed histogram of fractional linear polarization and the narrow width of the observed histogram of fractional circular polarization suggest the modes are highly linearly polarized, such that the colatitude of the modes' polarization vectors is  $\theta_o \simeq \pi/2$  (M02). The simulation of PSR B1929+10 is shown in the three panels on the right side of Figure 7. The model parameters used in the simulation are  $\mu_1 = 15.9$ ,  $\mu_2 = 3.7$ , and  $\theta_o = 88^\circ$ . The simulated position angle histogram is very similar to what is observed. The simulated histogram of fractional linear polarization spans its entire range with more samples at high linear polarization, just as equation 23 predicts when  $M$  is large and  $\theta_o \simeq \pi/2$ . The simulated histogram of fractional circular polarization is narrow with a large peak and slight asymmetry as predicted by equation 24. However, the simulated asymmetry is not quite as discernible as what is observed.

## 4. DISCUSSION

### 4.1. Comparison between Gaussian and Exponential Intensity Fluctuations

The distributions of the Stokes parameters I, Q, U, and V, linear polarization, fractional polarization, and position angle derived from Gaussian and exponential mode intensities have similarities and differences. Overall, the distributions of the Stokes parameters and fractional polarization are unimodal. This feature of the distributions is not a coincidence. It is a direct result of the statistical model's fundamental assumption that OPMs are superposed (M02). If the modes were disjoint, the resulting distributions would generally be bimodal because disjoint modes are mutually exclusive, i.e. when one mode is present, the other one is always absent (MS2; M02). OPMs could be fundamentally disjoint, but the switching timescale between them remains unresolved (van Straten & Tiburzi 2017).

When the mode intensities are exponential RVs, the distribution of the observed Stokes parameter I resembles a smoothed, one-sided exponential, and distributions of the observed Stokes parameters Q,

**Table 2.** Comparison of Properties of Position Angle Distributions

Mode Fluctuations	Exponential	Gaussian
Difference in Peak Amplitudes	$\sqrt{2/\pi}\mu_Q/\sigma$	$\sqrt{2/\pi}\mu_Q/\sigma$
Primary Mode Peak Width, FWHM	$\ln(2)\sigma/\mu_1$	$\arcsin(1/\rho) \exp[-\mu_Q/(k_1\sigma_Q)]$
Secondary Mode Peak Width, FWHM	$\ln(2)\sigma/\mu_2$	$\arcsin(1/\rho) \exp[\mu_Q/(k_2(\rho)\sigma_Q)]$

U, and V resemble smoothed, two-sided exponentials. These distributions are unimodal and generally *asymmetric*. The modulation index of the total intensity lies in the range  $0.71 \leq \beta \leq 1$ , comparable to what is commonly observed in pulsars (BSW). The distribution of linear polarization *always* resembles a Rician with an extended tail. The distribution flattens and the tail becomes longer as  $M$  increases. The distributions of fractional polarization are uniform when  $M = 1$  and gradually skew upwards towards high values of fractional polarization as  $M$  increases. The distribution of fractional circular polarization can become highly asymmetric when  $M$  is large. The distributions of fractional linear and fractional circular polarization are abruptly truncated at  $\sin \theta_o$  and  $\pm \cos \theta_o$ , respectively, because the fractional polarization of the combined emission can never exceed the degree of linear or circular polarization intrinsic to the individual modes. Instrumental noise smooths the cutoff, causing the distributions to peak near  $\sin \theta_o$  and  $\cos \theta_o$ . Accordingly, the extent of the fractional polarization in observed histograms can be used to constrain the ellipticity of the polarization intrinsic to the modes. The distribution of polarization position angle is generally bimodal, consisting of two peaks sitting atop a uniform plateau and separated by  $\pi/2$  radians (Figure 5). As shown in Table 2, the full width at half maximum (FWHM) of the peaks varies as  $\Delta\psi_j \simeq \ln(2)\sigma/\mu_j$ . The functional forms of the peak widths listed in the table were found by calculating the widths directly from the position angle distributions and approximating them with an equation that best represented the calculated values (see Figure 8). The FWHM of one mode peak is independent of the other mode. The secondary mode peak is generally wider than the primary mode peak, because  $\mu_2 \leq \mu_1$  by definition. The difference in the amplitudes of the peaks is directly proportional to the difference in mode mean intensities,  $\mu_Q = \mu_1 - \mu_2$  (Table 2).

When the mode intensities are Gaussian RVs, the Stokes parameters are also Gaussian RVs; therefore, their distributions are unimodal and *symmetric*. The modulation index of the total intensity lies in the range  $\beta \leq 0.2 - 0.3$ . The distributions of linear polarization and fractional polarization resemble a Rician with an extended tail when  $\mu_Q = 0$  ( $M = 1$ ; see equation 34 of McKinnon 2003), but evolve into single, isolated Gaussians as  $M$  increases (see MS1, Figure 1 and equations 12 and 16). The width of the distribution of fractional circular polarization varies roughly as the product of the emission's modulation index and the modes' degree of circular polarization,  $\beta \cos \theta_o$  (see equation 21 of M02). The position angle distributions derived from Gaussian RVs are similar to those derived for exponential RVs (compare Figure 5 with Figure 2 of MS1). Despite the differences in the statistical character of their fluctuations, the difference between mode peak amplitudes is the

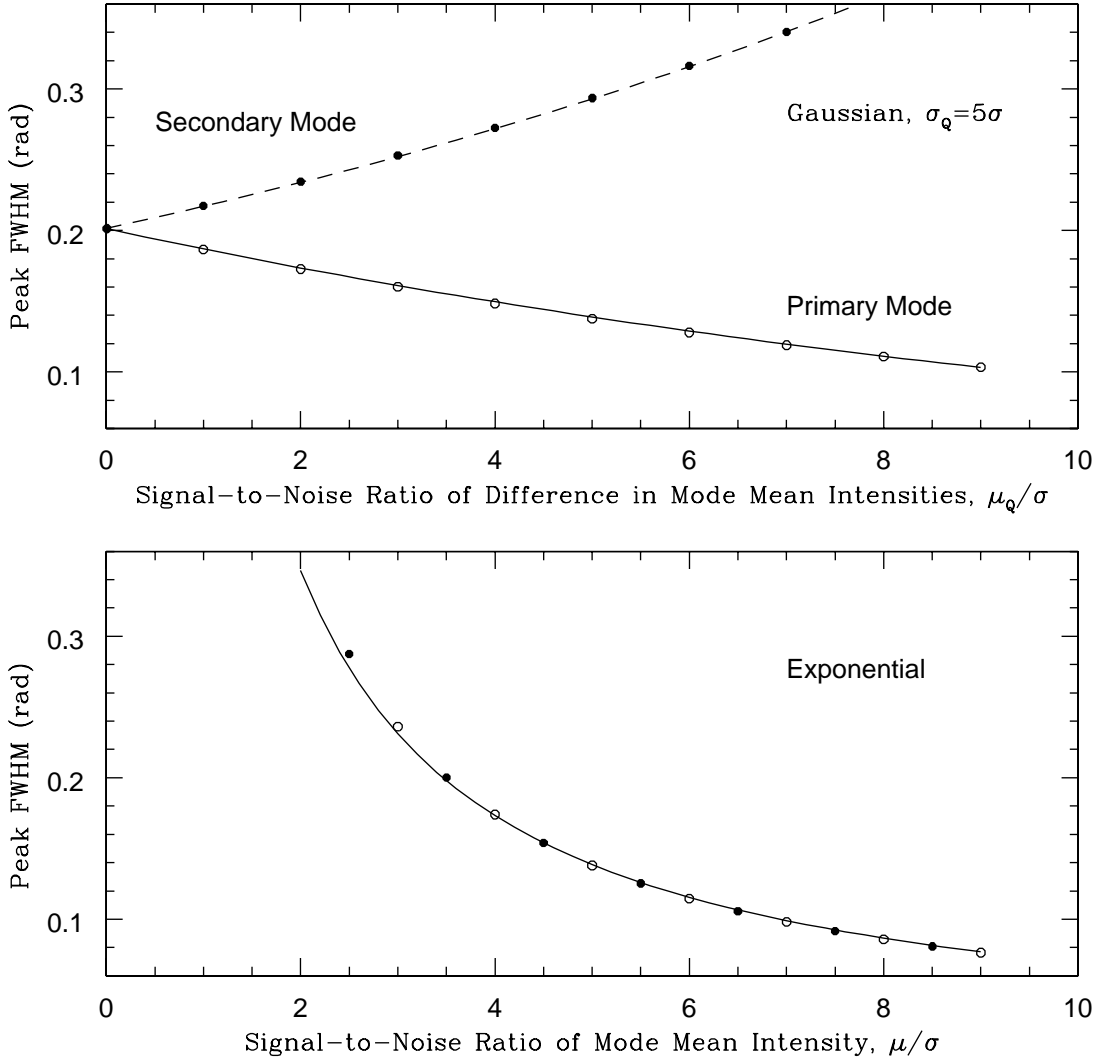


**Figure 8.** Widths of the mode peaks in the position angle distributions for Gaussian fluctuations (top panel) and exponential fluctuations (bottom panel) in mode intensities. For exponential fluctuations, the widths of both mode peaks follow the same track in varying with  $\mu_j$ . For Gaussian fluctuations, the widths of the primary mode peak (solid line) and secondary mode peak (dashed line) follow separate tracks in varying with  $\mu_Q$ . The data points in both panels represent the peak widths measured from the distributions. Open and closed circles denote the peak widths of the primary and secondary modes, respectively. The lines drawn in the panels are approximations to the data. Their analytical form is shown in Table 2. The constant values used in the figure are  $\sigma_Q = 5\sigma$ ,  $\sigma = 1$ ,  $k_1 = 2.692$ , and  $k_2(5) = 2.666$  (see Table 2).

same for exponential and Gaussian mode intensities (Table 2). The FWHM of the Gaussian mode peaks are dependent upon one another through  $\mu_Q$  and  $\sigma_Q$ . When  $\mu_Q = 0$ , both the amplitudes and widths of the two peaks are equal, with the FWHM of the peaks varying as  $\Delta\psi = \arcsin(\rho^{-1}) \simeq \rho^{-1}$ , where  $\rho = \sigma_Q/\sigma$  (see equation 38 of MS1). As  $\mu_Q$  increases, the width of the primary mode peak narrows exponentially, and the width of the secondary mode peak broadens exponentially (Table 2 and Figure 8). Thus, the secondary mode peak is generally wider than the primary mode peak.

When  $\mu_Q$  exceeds  $\sigma_Q$ , the width of the secondary mode peak becomes large, eventually merging into the distribution's noise floor, at which point the distribution features only the primary mode peak. The parameters  $k_1$  and  $k_2(\rho)$  used in the expressions for the FWHM of the Gaussian mode peaks in Table 2 were determined for multiple values of  $\rho$ . The value of  $k_1$  varied little with  $\rho$ , and is statistically consistent with a constant. The value of  $k_2(\rho)$  increases with  $\rho$ . The values used in the fits to the FWHM data points in Figure 8 are  $k_1 = 2.692$  and  $k_2(5) = 2.666$ .

#### 4.2. *Spectra of the Statistical Parameters*

The analysis of exponential mode intensities was used to derive parameters that quantify the statistical properties of the emission and its polarization. The analysis shows the parameters are dependent only on the mode intensity ratio,  $M$ , and are independent of the mean intensities of the individual modes. If the statistical model is a reasonable representation of the emission and if the fluctuations in mode intensities retain their exponential character over a wide range of frequency, the spectral behavior of the parameters should coevolve in frequency in accordance with the frequency dependence of  $M$  and their dependence upon  $M$ . For example, both the modulation index,  $\beta$ , and the fractional linear polarization,  $\bar{L}$ , of many pulsars are known to decrease with increasing frequency (BSW; Manchester, Taylor, & Huguenin 1973; Morris, Graham, & Seiber 1981). This behavior is qualitatively consistent with their dependence upon  $M$ , as listed in Table 1, and with  $M$  decreasing with increasing frequency. Similarly, Karastergiou et al. (2005) suggested the frequency dependence of a pulsar's fractional linear polarization depends upon the total intensity spectra of the two orthogonal modes, or alternatively the spectrum of the mode intensity ratio, provided the modes are completely polarized, as assumed in this analysis. As the mode intensities become comparable, the radiation will depolarize and the modes will occur with nearly equal frequency. Their simultaneous, dual-frequency observations showed this to be the case for PSR B1133+16 (Karastergiou et al. 2002).

#### 4.3. *Origin of the Mode Intensity Fluctuations*

The different types of mode intensity fluctuations evaluated within the context of the model's statistical framework suggest different interpretations for their physical origins. When MS1 evaluated the mode intensities as Gaussian RVs, the mode means were generally different, but their standard deviations were the same. Within the context of pulsar radio emission and OPMs, this scenario could arise from the birefringence of the pulsar's magnetospheric plasma (Melrose 1979; Allen & Melrose 1982). The extraordinary (X) mode propagates as if in vacuum along a straight ray path, so its trajectory is largely unaffected by the plasma. The ordinary (O) mode has a different index of refraction, and is ducted along the pulsar's open magnetic field lines (Onishchenko 1981; Barnard & Arons 1986). The birefringence of the plasma causes the modes to separate spatially, possibly resulting in the difference between their mean intensities ( $\mu_1 \neq \mu_2$ ) at specific locations within the pulse. The fluctuations in mode intensities could then be attributed to the underlying emission mechanism, where both modes would be modulated in a similar, but independent, way leading to  $\sigma_1 = \sigma_2$ .

The treatment of mode intensities as exponential RVs in this work requires the mode intensity fluctuations to be different ( $\sigma_1 \neq \sigma_2$ ) to explain what is observed. It seems difficult for a single emission mechanism to modulate the mode intensities differently. One possibility for the difference in mode intensity fluctuations is the modes are produced by separate emission mechanisms, such as the generation of the X-mode by curvature radiation and the generation of the O-mode by the

acceleration of charged particles along magnetic field lines, as proposed by Cheng & Ruderman (1979). Alternatively, the difference in mode fluctuations could arise from their different propagation or scattering properties. In this scenario, the intensities of both the X- and O-mode are fundamentally modulated by the underlying emission mechanism, but the O-mode intensity fluctuations are altered, for example, by stimulated scattering in the magnetosphere where an electron's gyrofrequency is very large in comparison to the frequency of a photon incident upon it (Blandford & Scharlemann 1976; Sincell & Krolik 1992; Lyubarskii & Petrova 1996). Scattering of the X-mode is comparatively negligible, so its fluctuations would be largely unaffected. Summarizing, differential refraction alone is not sufficient to explain the observed behavior of the orthogonal modes; their intensities must also fluctuate differently.

## 5. CONCLUSIONS

Distributions of the Stokes parameters and fractional polarization of pulsar radio emission were derived from a statistical model assuming the intensities of the orthogonal modes comprising the emission are exponential random variables. The analysis incorporates both linear and circular polarization and accounts for instrumental noise. The resulting distributions of the Stokes parameters and fractional polarization are unimodal, as found when the mode intensities follow Gaussian statistics. This general feature of the distributions arises from the fundamental assumption that the modes are superposed, and is generally consistent with what is observed. However, unlike the symmetric distributions produced from Gaussian mode intensities, the distributions produced by exponential mode intensities are generally asymmetric. Distributions of the emission's fractional polarization are truncated at the degree of linear and circular polarization intrinsic to the modes. The asymmetric distributions have been observed in single pulse polarization observations of pulsars. Additionally, exponential mode statistics can replicate the heavy modulation of the intensity and polarization observed in the emission, whereas Gaussian statistics cannot. The position angle distributions derived from exponential and Gaussian mode fluctuations are similar in appearance. The width of an exponential mode peak in the distribution is independent of the other mode, while the widths of the Gaussian mode peaks are dependent upon one another. The analysis also shows that a number of observables, such as modulation index, mode frequency of occurrence, and mean fractional polarization, are functions only of the ratio of mode mean intensities,  $M$ , suggesting their spectral evolution is determined primarily by the frequency dependence of  $M$ . If the statistical model with its implementation of exponential mode intensities is a plausible explanation for the polarization of pulsar radio emission, some type of mechanism must be responsible for causing different fluctuations in the intensities of the orthogonal modes. Since fluctuations produced by a single emission mechanism would presumably affect both modes similarly, the difference in mode fluctuations could arise from different emission mechanisms for the modes or from mode-dependent propagation or scattering effects within the pulsar magnetosphere.

## APPENDIX

### A. JOINT PROBABILITY DENSITY AND FRACTIONAL POLARIZATION

The joint probability density of  $Q$  and  $I$  must be found to derive the distribution of fractional linear polarization. In the derivation of MS1,  $Q$  and  $I$  were constructed to be independent, which is

appropriate for the Gaussian RVs used in their analysis, but not for the exponential RVs considered here. From Ross (1984), the joint probability density of two functions,  $y_1$  and  $y_2$ , of two random variables,  $x_1$  and  $x_2$ , can be found from

$$f_{Y_1 Y_2}(y_1, y_2) = f_{X_1 X_2}(x_1, x_2) |J(x_1, x_2)|^{-1} \quad (\text{A1})$$

where  $f_{X_1 X_2}(x_1, x_2) = f_{X_1}(x_1) f_{X_2}(x_2)$  is the joint probability density of the independent RVs  $x_1$  and  $x_2$ , and the matrix  $J$  is the Jacobian given by

$$J(x_1, x_2) = \begin{pmatrix} \partial y_1 / \partial x_1 & \partial y_1 / \partial x_2 \\ \partial y_2 / \partial x_1 & \partial y_2 / \partial x_2 \end{pmatrix}. \quad (\text{A2})$$

From equations 5 and A1, the joint probability density of  $I = y_1 = x_1 + x_2$  and  $Q = y_2 = x_1 - x_2$  is

$$f_{QI}(y_1, y_2) = \frac{1}{2\mu_1\mu_2} \exp\left[-\frac{y_1(\mu_1 + \mu_2)}{2\mu_1\mu_2}\right] \exp\left[\frac{y_2(\mu_1 - \mu_2)}{2\mu_1\mu_2}\right]. \quad (\text{A3})$$

The cumulative distribution of the fractional linear polarization,  $F_m(z)$ , is the probability that  $|Q/I| \leq z$  (MS1).

$$F_m(z) = P\{|Q/I| \leq z\} = P\{-z \leq Q/I \leq z\} = F_{Q/I}(z) - F_{Q/I}(-z) \quad (\text{A4})$$

$$F_m(z) = \int_0^\infty \int_{-\infty}^{y_1 z} f_{QI}(y_1, y_2) dy_2 dy_1 - \int_0^\infty \int_{-\infty}^{-y_1 z} f_{QI}(y_1, y_2) dy_2 dy_1 \quad (\text{A5})$$

The cumulative distribution of the fractional linear polarization for the specific case of exponentially distributed mode intensities is found by completing the above integrals using the joint probability density of  $I$  and  $Q$  from equation A3.

$$F_m(z) = \frac{(1 - m^2)z}{1 - m^2 z^2} \quad (\text{A6})$$

The distribution of fractional polarization given by equation 11 is then found by taking the derivative of the cumulative probability density.

$$f_m(z) = \frac{dF_m}{dz} \quad (\text{A7})$$

## ACKNOWLEDGMENTS

The National Radio Astronomy Observatory is a facility of the National Science Foundation operated under cooperative agreement by Associated Universities, Inc.

## REFERENCES

- |  |   |
|--|---|
| Allen, M. C. & Melrose, D. B. 1982, Proc. Astron. Soc. Aust., 4, 365 | Bartel, N., Sieber, W., & Wolszczan, A. 1980, A&A, 90, 58 (BSW) |
| Barnard, J. J. & Arons, J. 1986, ApJ, 302, 138                       | Blandford, R. D. & Scharlemann, E. T. 1976, MNRAS, 174, 59      |

- Chandrasekhar, S. 1960, Radiative Transfer, (New York: Dover)
- Cheng, A. F. & Ruderman, M. A. 1979, ApJ, 229, 348
- Cordes, J. M., Rankin, J. M., & Backer, D. C. 1978, ApJ, 223, 961 (CRB)
- Karastergiou, A., Kramer, M., Johnston, S., Lyne, A. G., Bhat, N. D. R., & Gupta, Y. 2002, A&A, 391, 247
- Karastergiou, A., Johnston, S., & Manchester, R. N. 2005, MNRAS, 359, 481
- Lyubarskii, Y. E. & Petrova, S. A. 1996, Astron. Let. 22, 399
- Manchester, R. N., Taylor, J. H., & Huguenin, G. R. 1973, ApJ, 179, L7
- Manchester, R. N., Taylor, J. H., & Huguenin, G. R. 1975, ApJ, 196, 83
- Melrose, D. B. 1979, Aust. J. Phys., 32, 61
- McKinnon, M. M. 2002, ApJ, 568, 302 (M02)
- McKinnon, M. M. 2003, ApJS, 148, 159
- McKinnon, M. M. 2004, ApJ, 606, 1154 (M04)
- McKinnon, M. M. 2014, PASP, 126, 476 (M14)
- McKinnon, M. M. & Stinebring, D. R. 1998, ApJ, 502, 883 (MS1)
- McKinnon, M. M. & Stinebring, D. R. 2000, ApJ, 529, 435 (MS2)
- Morris, D., Graham, D. A., & Sieber, W. 1981, A&A, 100, 107
- Onishchenko, O. G., 1981, Sov. Astron. Lett., 7, 404
- Ross, S. 1984, A First Course in Probability, (New York: Macmillan), 217
- Sincell, M. W. & Krolik, J. H. 1992, ApJ, 395, 553
- Stinebring, D. R., Cordes, J. M., Rankin, J. M., Weisberg, J. M., & Boriakoff, V. 1984a, ApJS, 55, 247 (S84a)
- Stinebring, D. R., Cordes, J. M., Weisberg, J. M., Rankin, J. M., & Boriakoff, V. 1984b, ApJS, 55, 279 (S84b)
- van Straten, W. & Tiburzi, C., 2017, ApJ, 835, 293